JMEPEG (2019) 28:169–182
https://doi.org/10.1007/s11665-018-3784-x

1059-9495/$19.00

Experimental Investigations for Optimizing the Extrusion Parameters on FDM PLA Printed Parts

Leipeng Yang, Shujuan Li, Yan Li, Mingshun Yang, and Qilong Yuan

(Submitted March 6, 2018; in revised form July 12, 2018; published online December 17, 2018)

Fused deposition modeling (FDM) has become one of the most extensively used additive manufacturing technologies in recent years because of its wide adaptability, simple mechanism and low cost. It is difficult, however, to achieve an equitable trade-off among mechanical properties, surface finish quality and production time, which is an area seldom explored. This paper concentrates on the optimization of the parameters to achieve higher tensile strength and lower surface roughness with less build time during the FDM process based on central composite design for the tensile specimen forming process. The effects of five extrusion parameters (nozzle diameter, liquefier temperature, extrusion velocity, filling velocity and layer thickness) on the three outputs of tensile strength (TS), surface roughness (SR) and build time (BT) are investigated. Response surface methodology combined with nondominated sorting genetic algorithm II is developed to optimize the process parameters to achieve the maximum TS, minimum SR and BT, as verified by subsequent experiments. The predicted results are found to be very close to the experimental data, illustrating that the presented approach in this paper is effective for improving mechanical properties, surface finish and efficiency of the FDM process.

Keywords build time, fused deposition modeling, multiobjective optimization, response surface methodology, surface roughness, tensile strength

1. Introduction

In recent years, additive manufacturing (AM) has aroused widespread public concern (Ref 1). AM technologies typically fall into two categories: One involves altering the state of the material by temperature change, such as fusion deposition modeling (FDM) (Ref 2), stereolithography (SLA) (Ref 3) and selective laser sintering (SLS) (Ref 4); and the other involves the bonding of material together through an adhesive, for example, 3D printing (3DP) (Ref 5) and laminated object manufacturing (LOM) (Ref 6). Because of its capability of free forming, the FDM process is used for a series of functions, including but not limited to prototyping, modeling and production applications. In the FDM process, a solid model of a desired part is developed and saved as a STL file and is sliced and input into a FDM machine. On this basis, the nozzle head of FDM moves horizontally and vertically to form the required three-dimensional parts directly. The filament material is preheated and extruded through the nozzle onto the platform. The deposited material is cooled, solidified and bonded with the surrounding materials. After the accomplishment of one layer, the platform drops one layer, and the procedure is repeated layer by layer until the part is built. As a result of the selection of multiple process parameters and the microstructural anisotropy caused by the layer-by-layer effect of the building procedure, the mechanical properties and the surface quality of the final forming part by FDM are lower than those made by traditional manufacturing processes. Two methods to overcome the limitation have been proposed: One method is to achieve good mechanical properties by exploiting new materials; and the other is to enhance mechanical performance and surface quality by adjusting and optimizing the technological parameters (Ref 7, 8).

In the literature, several researchers have been focused on the adjustment of the FDM process parameters to optimize the quality characteristics. Wang et al. (Ref 9) studied the impacts of several significant process variables on dimensional accuracy, surface roughness and tensile strength of acrylonitrile–butadiene–styrene (ABS) copolymers part and obtained the optimum parameter combination. Zhang et al. (Ref 10) investigated the effects of process variables (including wire-width compensation, extrusion velocity, filling velocity and layer thickness) on the dimensional error and deformation of a FDM-processed ABS prototype through the Taguchi method integrated with fuzzy comprehensive evaluation. Sood et al. (Ref 11) found that the layer thickness and the raster angle remarkably affect the residual stress and deformation compared to other controllable factors by CCD combined with an ANOVA. Rayegani et al. (Ref 12), adopting a method of full factorial design, GMDH and DE, also suggested that build orientation, air gap, raster angle and width influence the tensile strength of the FDM prototype. The optimum technological parameters of the maximum tensile strength were obtained. Hossain et al. (Ref 13) focused on the improvement of ultimate tensile strength, Young's modulus and tensile strain by modifying the process parameters. The results showed that air gap removal has a significant effect on the mechanical properties. Peng et al. (Ref 14) applied RSM combined with the fuzzy inference system to investigate the effects of process variables such as line width compensation, extrusion velocity, filling velocity, and layer thickness on both manufacturing

Leipeng Yang, Shujuan Li, Yan Li, Mingshun Yang, and **Qilong Yuan**, School of Mechanical and Precision Instrument Engineering, Xi'an University of Technology, 5 South Jinhua Road, Xi'an, 710048 Shaanxi, China. Contact e-mail: shujuanli@xaut.edu.cn.

accuracy and efficiency. The application of FIS, however, requires adequate professional knowledge and experience. Dawoud et al. (Ref 15) suggested that an adequate selection of FDM parameters is able to achieve mechanical properties that are comparable to those of injection molded parts in both static and dynamic loading modes. Torres et al. (Ref 16) reported the influence of some important parameters on the mechanical properties of FDM-processed PLA prototype; in particular, a slower speed and lower layer thickness led to a higher resolution with an improved surface quality. Panda et al. (Ref 17) performed a demanding multiobjective optimization of the fabricating precision and quality using an evolutionary system identification method and found that the layer thickness and extrusion speed have an effect on the warpage. Moreover, the filling velocity and line width compensation affect the dimensional error the most. Singh (Ref 18) studied and optimized the processing parameters of single-screw extruder fabricated ABS parts and the mathematical models of tensile strength. Young's modulus and the deviation were also determined, and optimized settings of the screw extruder parameters were obtained. Mohamed (Ref 19) developed mathematical models to predict the process time, material cost and mechanical performance and found that the most effective variables were layer thickness, air gap, build direction, etc. Vahabli (Ref 20) built a specific test piece to evaluate the surface quality distribution for mutative build angles based on the RBFNN-ICA model.

Most of the studies in the literature focus on the effect of FDM process parameters, such as layer thickness, air gap, road width, number of contours, raster angle and orientation. Nevertheless, some significant parameters have not been studied, for example, nozzle diameter and liquefier temperature. Regarding the material properties, the great majority of the research studies concentrated on optimization of the technical parameters for an ABS part. In contrast, there are very few studies on other FDM process material. Moreover, in practical applications, the parameters require adjustment to take into account the mechanical properties, surface finish and production time simultaneously. This paper focuses on a polylactic acid (PLA) filament study. CCD is applied to investigate the influence of the major extrusion parameters, including nozzle diameter, liquefier temperature, extrusion velocity, filling velocity and layer thickness, on the tensile strength, surface roughness and build time. Furthermore, on the basis of an empirical model from response surface methodology, the optimal combination of process parameters is obtained by performing multiobjective optimization on the tensile strength, surface roughness and build time using the NSGA-II algorithm.

2. Experimental Process

2.1 Parameter Modifications

In this study, five extrusion parameters are included for investigation; their ranges and levels, which are defined on the basis of the literature review, industrial experience, and the approved low and high levels suggested by the device manufacturers, are listed in Table 1. Other constant factors are listed in Table 2. This study considered the new variables of 'nozzle diameter' and 'liquefier temperature.' The levels of these factors are defined as follows:

1. Nozzle diameter: Nozzle diameter refers to the internal diameter of the nozzle terminal.
2. Liquefier temperature: It is the operating temperature of the nozzle heating unit at which the filament starts to melt and flow.
3. Extrusion velocity: It is the speed that the filament is extruded through the preheated injector, based on the material feeding pressure and speed.
4. Filling velocity: Filling velocity refers to the moving velocity of the nozzle, namely, molding speed.
5. Layer thickness: It is the height of one layer sliced by the layered software.

As shown in Fig. 1, the filament amount of nozzle extrusion is equal to the quantity of deposition at the same time. Therefore, the deposition width can be calculated as follows:

$$\pi\left(\frac{D_N}{2}\right)^2 V_E = \pi\left(\frac{\omega}{2}\right)\left(\frac{H_L}{2}\right)V_F \quad \text{(Eq 1)}$$

where D_N is the nozzle diameter, V_E is the extrusion velocity, V_F is the filling velocity, H_L is the layer thickness, and ω is the deposition width.

Table 2 The values of the fixed factors

Fixed factor	Value	Unit
Build orientation	0	°
Filament diameter	1.75	Mm
Envelop temperature	50	°C
Air gap	0	Mm
Filling rate	100	%
Part filling style	Perimeter/raster	…
Number of contours	5	…

Table 1 The controllable factors and levels

Factor	Symbol	Level			Unit
		Low (− 1)	Center (0)	High (1)	
Nozzle diameter	A	0.2	0.4	0.6	Mm
Liquefier temperature	B	200	215	230	°C
Extrusion velocity	C	20	25	30	mm/s
Filling velocity	D	20	30	40	mm/s
Layer thickness	E	0.1	0.2	0.3	mm

2.2 Experimental Equipment

All test specimens are fabricated using Raise3D N2 plus in this work. Figure 2 shows the tensile specimen size diagram based on the ISO 527-1:2012 standard (Ref 21). The tensile strength is measured by HT-2402 Computer Servo Control Material Testing Machines produced by Hung Ta Instrument Co., Ltd. The model material used in each test piece is PLA, which is a biodegradable thermoplastic polymerized from natural sources, such as corn. Some of the characteristics of PLA are given in Table 3 by the manufacturer Polymaker (Ref 22). In addition, the microstructures of the specimens and fracture surfaces were determined using a Keyence VHX-5000 digital microscope.

Ra is the most widely used parameter for evaluating surface roughness. In this paper, the value for Ra of the upper surface of the specimen was measured using a TR300 roughness meter produced by Beijing TIME High Technology Ltd. To minimize the error, the five measurements are averaged to represent the surface roughness of each specimen. Moreover, the build time, which is the total time from the start of the nozzle heating at the initial position to the return after fabricating completion, is the main manufacturing cost.

2.3 Design of Experiment and Responses

As an empirical modeling method, RSM is adopted to study the internal relations of process variables and to build a mathematical model that can precisely represent the overall process. To develop an empirical model for tensile strength, surface roughness and process time and investigate the effects of the process factors on them, experiments were implemented in accordance with CCD. The specific experimental scheme and results obtained for every experimental run were estimated to build the best fitted empirical models, as shown in Table 4.

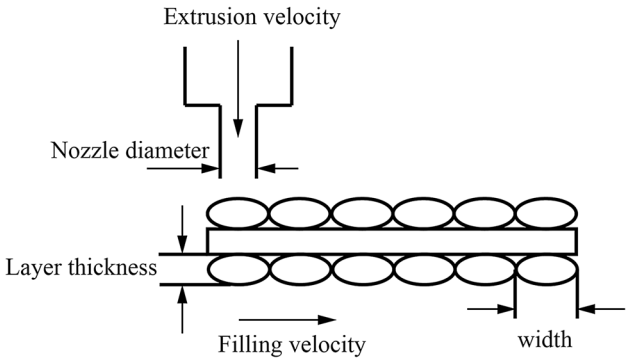

Fig. 1 Schematic representation of the extrusion parameters

3. Results and Discussion

On the basis of the experimental results shown in Table 4, further investigations were launched to study the effects of each variable on three responses mentioned above. On this foundation, the functional relationships of three responses were fitted individually by using response surface methodology, and a quadratic model was taken in this study:

$$y = \beta_0 + \beta_i \sum_{i=1}^{n} x_i x_j + \beta_{ij} \sum_{i<j} x_i x_j + \beta_{ii} \sum_{i=1}^{n} x_i^2 + \varepsilon \qquad \text{(Eq 2)}$$

where y is the response, x_i is a factor, β_i is a linear coefficient, and β_{ii} is a quadratic coefficient.

3.1 Tensile Strength

An ANOVA is employed to evaluate the fitness of the model and to estimate the significance of each factor to the response. The ANOVA results of tensile strength are listed in Table 5. The 95% level of confidence means the factor effect is identified as significant to the response in the situation, and the corresponding P value is less than or equal to 0.05. From Table 5, the P value of the model is less than 0.0001, which indicates the satisfactory fitness of the established quadratic model.

Table 3 The characteristics of PLA

Property	Unit	Value
Density	g/cm^3	1.24
Glass transition temperature	°C	60
Melt index	g/10-min	11
Young's modulus	MPa	2636
Tensile strength	MPa	46.6
Elongation at break	%	1.9

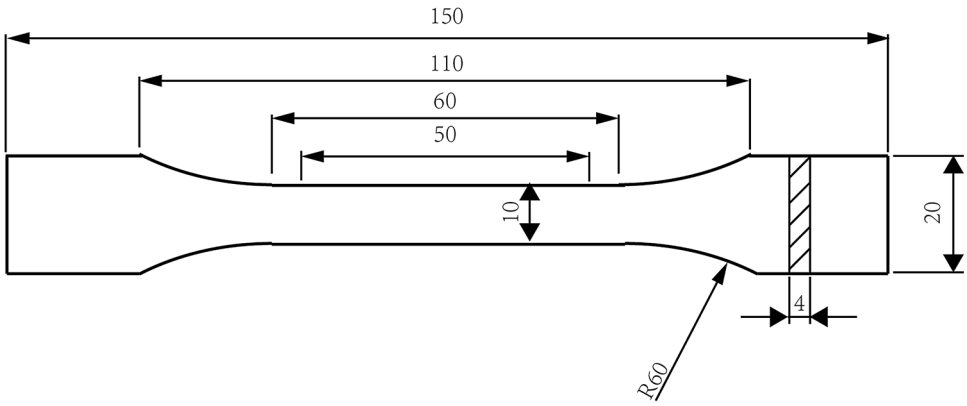

Fig. 2 Schematic representation of the tensile specimen

Table 4 Experimental scheme and results

	Factors					Responses		
Exp. No.	A, mm	B, °C	C, mm/s	D, mm/s	E, mm	Tensile strength, MPa	Surface roughness *Ra*, μm	Build time, h
1	0.4	215	20	30	0.2	38.442	20.69	1.41
2	0.4	200	25	30	0.2	40.274	22.35	1.45
3	0.2	200	20	20	0.1	31.628	6.16	6.23
4	0.2	200	30	20	0.3	35.061	19.67	2.89
5	0.2	230	30	20	0.1	35.879	9.27	6.13
6	0.4	215	25	30	0.2	42.192	22.52	1.37
7	0.4	215	25	30	0.2	41.284	22.32	1.39
8	0.2	230	20	20	0.1	30.831	6.03	6.16
9	0.4	215	25	30	0.2	41.765	22.19	1.38
10	0.2	200	20	20	0.3	35.569	15.37	2.83
11	0.4	215	25	30	0.2	41.412	22.41	1.34
12	0.2	215	25	30	0.2	37.241	9.96	2.78
13	0.2	230	20	20	0.3	36.672	15.46	2.71
14	0.6	230	30	20	0.1	43.022	27.97	2.26
15	0.6	200	20	40	0.1	36.163	28.72	1.22
16	0.2	230	20	40	0.1	30.419	12.76	3.67
17	0.6	230	20	20	0.1	36.394	24.72	2.26
18	0.2	200	20	40	0.1	31.834	12.74	3.80
19	0.4	215	25	30	0.2	41.216	22.56	1.41
20	0.4	215	25	30	0.2	41.208	22.24	1.39
21	0.2	230	30	20	0.3	39.712	19.56	2.69
22	0.6	200	20	20	0.3	41.986	38.59	0.99
23	0.2	200	30	40	0.1	32.766	14.73	3.81
24	0.6	200	30	40	0.3	42.075	50.29	0.86
25	0.2	230	30	40	0.3	38.468	29.62	1.59
26	0.2	230	30	40	0.1	34.645	14.68	3.70
27	0.6	230	20	40	0.3	41.032	47.62	0.68
28	0.6	200	30	20	0.1	41.719	27.98	2.41
29	0.2	200	30	20	0.1	33.261	9.26	6.22
30	0.6	200	20	20	0.1	36.908	24.86	2.39
31	0.2	200	30	40	0.3	35.194	29.84	1.68
32	0.6	200	20	40	0.3	39.532	47.27	0.79
33	0.6	230	30	40	0.3	45.827	50.32	0.74
34	0.4	215	25	30	0.3	43.171	28.29	0.98
35	0.4	215	25	30	0.1	37.273	13.78	2.82
36	0.6	230	30	40	0.1	43.019	30.74	1.21
37	0.2	200	20	40	0.3	35.902	26.51	1.63
38	0.4	215	25	20	0.2	41.108	26.56	2.24
39	0.4	215	25	40	0.2	40.121	33.42	1.02
40	0.6	230	20	20	0.3	41.086	38.78	0.87
41	0.4	215	30	30	0.2	42.186	23.93	1.46
42	0.4	215	25	30	0.2	41.833	22.24	1.42
43	0.6	215	25	30	0.2	44.761	29.78	0.52
44	0.6	230	20	40	0.1	37.172	28.54	1.08
45	0.4	215	25	30	0.2	40.934	22.19	1.45
46	0.6	230	30	20	0.3	46.074	42.96	0.87
47	0.6	200	30	20	0.3	42.148	42.82	1.01
48	0.2	230	20	40	0.3	36.136	26.81	1.53
49	0.4	230	25	30	0.2	41.655	22.65	1.29
50	0.6	200	30	40	0.1	39.013	30.71	1.30

Figure 3 shows that the distribution of points tends to be linear in the normal probability plot of the residual for the response of tensile strength, i.e., the results have no large deviations. In addition, the model prediction ability is commonly measured by the value of predicted R^2, and the value R^2 of 0.9837 indicates that a model that provides more matching predictions can be widely used experimentally in further studies.

Because of the diversity of measurement scales and units from variables, the obtained model is not able to analyze the impacts of each variable on response correctly. Accordingly, the tensile strength model is obtained from the employment of coded parameter values and the elimination of insignificant factors, as presented in Eq 3. From the *F*-value in Table 5 and coefficient in Eq 3, all the five factors have remarkable linear effects, especially the nozzle diameter (*A*). Moreover, two level

Table 5 The ANOVA for the tensile strength

Source	SS	DF	MS	*F*-value	*P* value	Remarks
Model	727.72	20	36.39	87.43	< 0.0001	Significant
A	334.93	1	334.93	804.77	< 0.0001	Significant
B	21.46	1	21.46	51.56	< 0.0001	Significant
C	80.64	1	80.64	193.77	< 0.0001	Significant
D	2.79	1	2.79	6.7	0.0149	Significant
E	119.34	1	119.34	286.75	< 0.0001	Significant
A^2	0.33	1	0.33	0.78	0.3839	
B^2	0.39	1	0.39	0.95	0.3385	
C^2	2.73	1	2.73	6.55	0.016	Significant
D^2	1.39	1	1.39	3.34	0.0781	
E^2	3.22	1	3.22	7.75	0.0094	Significant
AB	0.2	1	0.2	0.48	0.4928	
AC	8.64	1	8.64	20.76	< 0.0001	Significant
AD	0.16	1	0.16	0.38	0.5415	
AE	0.81	1	0.81	1.95	0.1728	
BC	19.83	1	19.83	47.64	< 0.0001	Significant
BD	0.25	1	0.25	0.61	0.4413	
BE	2.79	1	2.79	6.71	0.0149	Significant
CD	0.28	1	0.28	0.67	0.4201	
CE	7.34	1	7.34	17.65	0.0002	Significant
DE	6.87E−03	1	6.87E−03	0.017	0.8986	
Residual	12.07	29	0.42			
Lack of fit	10.87	22	0.49	2.89	0.0767	
Total	739.79	49				

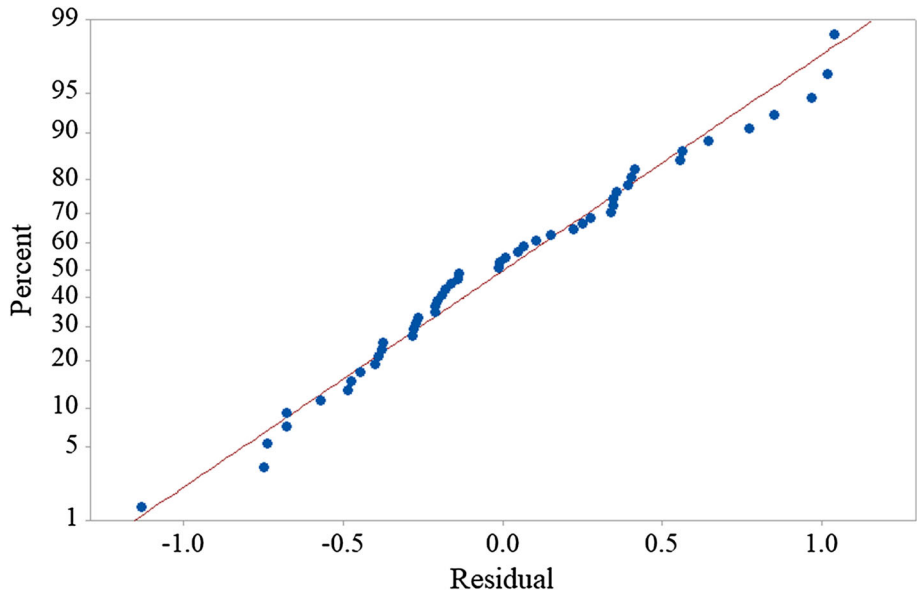

Fig. 3 Normal probability plot of the residuals for the tensile strength

interaction effects of liquefier temperature and extrusion velocity (*BC*) have significant influence on the tensile strength.

$$\begin{aligned} TS = {} & 41.32 + 3.14A + 0.79B + 1.54C - 0.29D \\ & + 1.87E - 1.73C^2 - 1.82E^2 + 0.52AC \\ & + 0.79BC + 0.3BE - 0.48CE \end{aligned} \quad \text{(Eq 3)}$$

As shown in Fig. 4, the interaction effects plot shows the second-order interaction between the parameters and their influence on tensile strength (TS). According to the first column of Fig. 4 and specimens 50 and 23 in Fig. 5, the tensile strength increases with the increase in the nozzle diameter because a larger nozzle diameter corresponds to a lower number of sliced layers for the same height of the part and the number of cooling and heating cycles is also reduced, resulting in distortion, delamination and fabrication failure of the build parts. Figure 6 shows that the fracture surface of specimen 50 is smoother than that of specimen 23. In previous research work, Bayraktar (Ref 23) generated a mathematical model for the tensile results using an ANN. On the basis of the model, the tensile strength values of most of the samples were observed to improve with a rise in liquefier temperature. The same variation is obviously observed

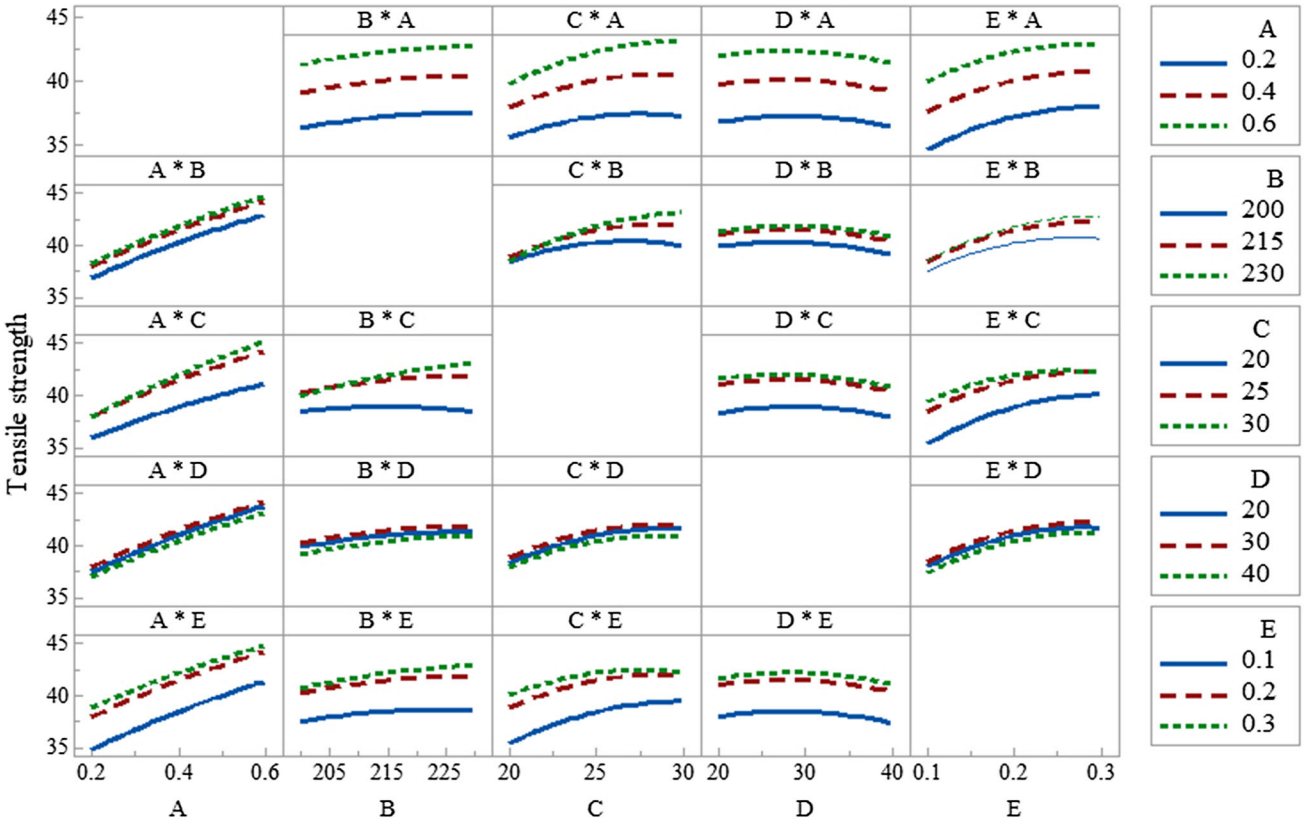

Fig. 4 The influence of parameter interaction on the tensile strength

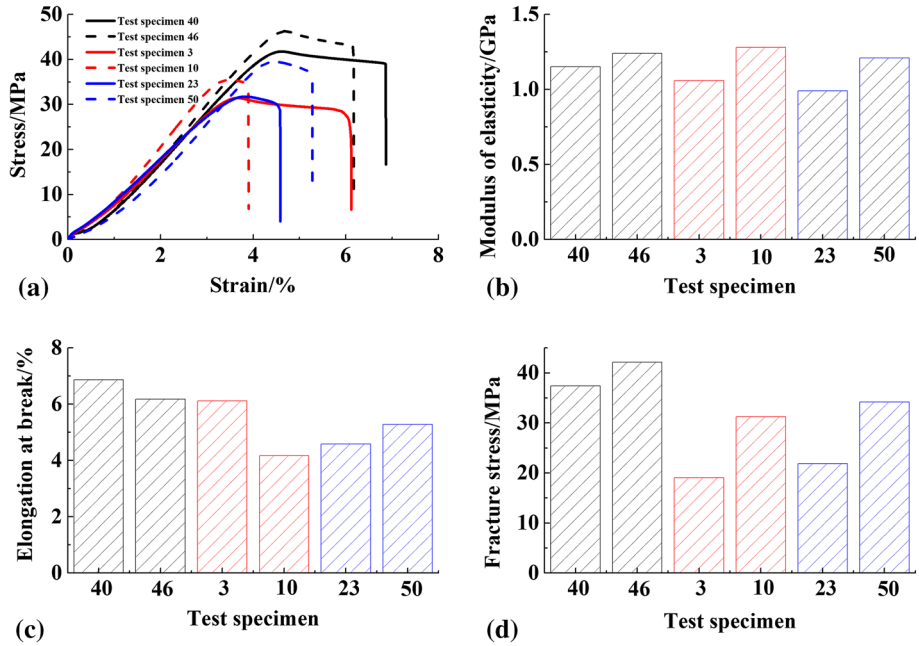

Fig. 5 (a) Representative stress–strain plots, (b) modulus of elasticity, (c) elongation at break and (d) fracture stress for typical specimens

in the second column of Fig. 4 because of the lower levels of molecular diffusion as well as the inability to form high numbers of cross-linked molecular bonds. Compared to that of specimen 30 in Fig. 6, the fracture surface of specimen 17 is smoother, and there is no obvious gap and crack, indicating that the higher liquefier temperature is beneficial to the adhesion between the layers. Similar to the liquefier temperature, as the extrusion velocity increases, the tensile strength increases because an increase in the extrusion velocity allows more force to be available to push the material from the die, leading to complete adhesion between layers, as shown in Fig. 6(e). Otherwise, slower extrusion velocity results in small holes

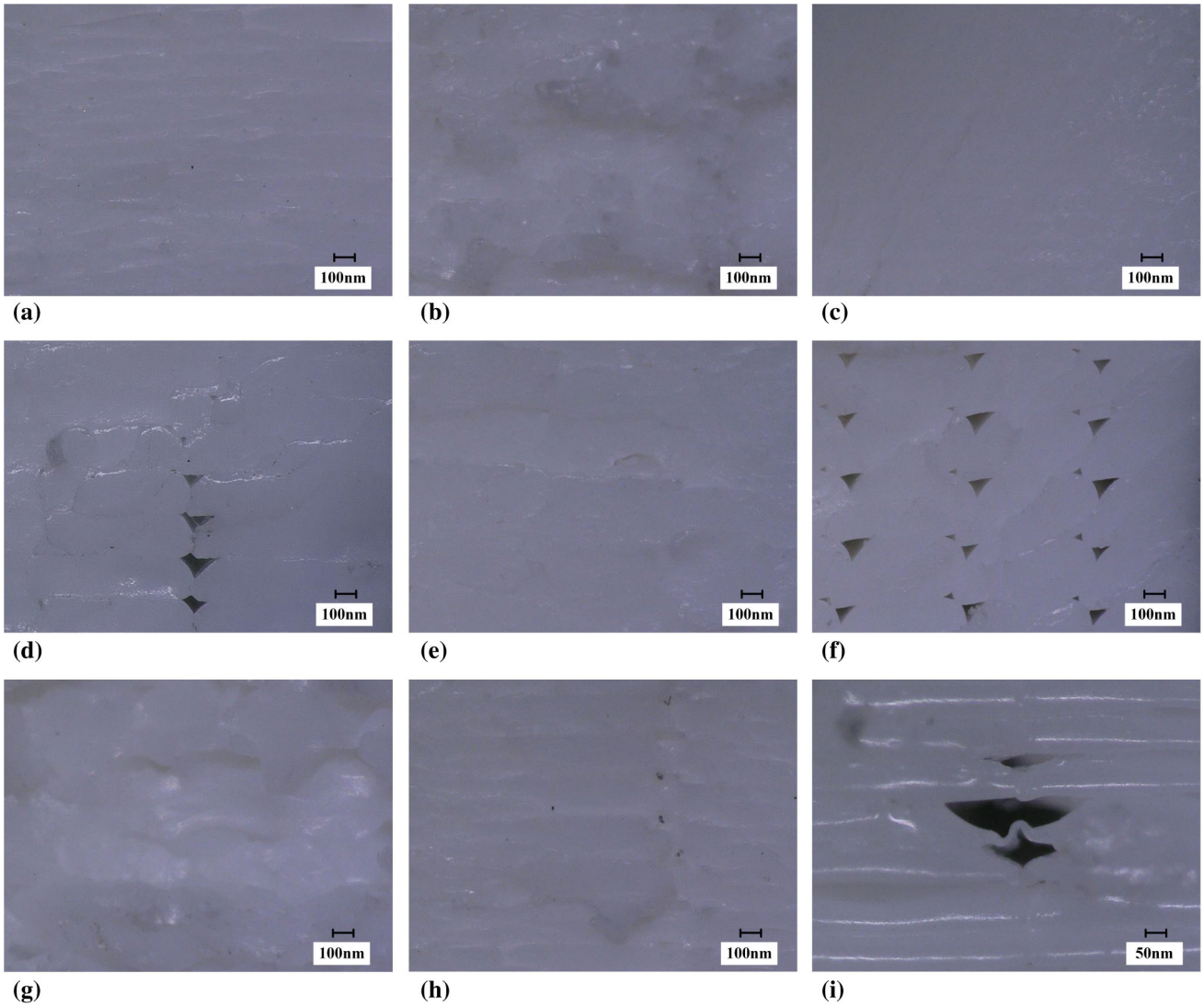

Fig. 6 The fracture surface microstructures of (a) specimen 50, (b) specimen 23, (c) specimen 17, (d) specimen 30, (e) specimen 46, (f) specimen 40, (g) specimen 10, (h) specimen 3 and (i) the microstructure of specimen 16

between layers, as it is seen from Fig. 6(f). This sort of incomplete filling will lead to a decrease in tensile strength. In contrast to the extrusion velocity, as displayed in the fourth column of Fig. 4, the tensile strength is insensitive to the filling speed. The tensile strength decreases slightly as the filling speed increases, possibly because of the discontinuous filament feeding, as shown in Fig. 6(i). Six FDM process parameters were studied to evaluate their effects on tensile strength by using the fraction factorial design and ANOVA (Ref 7). It was concluded that the layer thickness has a remarkable impact on tensile strength: as the layer thickness increases, the tensile strength increases, and the same variation is obviously observed in the fifth column of Fig. 4 and specimens 3 and 10 in Fig. 5. With the increase in the layer thickness, the number of layers required for the manufacturing parts decreases, resulting in minimum deformation and heat cycles and thus improving the dynamic mechanic performances of the parts. Comparing Fig. 6(g) with Fig. 6(h), the fracture surface of the thinner layer thickness has more obvious gaps and cracks and thus has a negative effect on the tensile strength.

3.2 Surface Roughness

The ANOVA results of surface roughness resemble the former analysis of tensile strength, as listed in Table 6. The level of confidence is 95%. From Table 6, the P value of the entire model is less than 0.0001, which indicates that the established quadratic model is sufficiently adequate. In Fig. 7, the normal probability plot of the residual for the response of surface roughness has no large deviations. For the value of R^2, the predicted coefficient of 0.9923 indicates a decent estimate in the experiments.

The surface roughness model with coded parameter values is obtained in Eq 4 by eliminating insignificant factors. From the F-value in Table 6 and the coefficient in Eq 4, the nozzle diameter, extrusion velocity, filling velocity and layer thickness have remarkable linear effects. The identical matching with the results shown in Eq 4 suggests that the nozzle diameter has the greatest influence on the surface roughness. Moreover, the quadratic effect of the filling velocity (B^2) and the two level interaction effects of nozzle diameter and layer thickness (AE)

Table 6 The ANOVA for the surface roughness

Source	SS	DF	MS	*F*-value	*P* value	Remarks
Model	5535.63	20	276.78	187.81	< 0.0001	Significant
A	3077.06	1	3077.06	2087.9	< 0.0001	Significant
B	0.023	1	0.023	0.015	0.9019	
C	155.71	1	155.71	105.65	< 0.0001	Significant
D	291.59	1	291.59	197.86	< 0.0001	Significant
E	1740.02	1	1740.02	1180.67	< 0.0001	Significant
A^2	44.37	1	44.37	30.1	< 0.0001	Significant
B^2	0.36	1	0.36	0.24	0.6265	
C^2	1.47	1	1.47	0.99	0.327	
D^2	154.94	1	154.94	105.13	< 0.0001	Significant
E^2	10.96	1	10.96	7.44	0.0107	Significant
AB	1.24	1	1.24	0.84	0.3658	
AC	0.5	1	0.5	0.34	0.5657	
AD	7.36	1	7.36	5	0.0333	Significant
AE	14.65	1	14.65	9.94	0.0037	Significant
BC	0.77	1	0.77	0.52	0.475	
BD	0.1	1	0.1	0.071	0.7918	
BE	1.24	1	1.24	0.84	0.3658	
CD	0.16	1	0.16	0.11	0.7455	
CE	6.73	1	6.73	4.56	0.0412	Significant
DE	1.11	1	1.11	0.75	0.3934	
Residual	42.74	29	1.47			
Lack of fit	36.06	22	1.64	1.72	0.2366	
Total	5578.37	49				

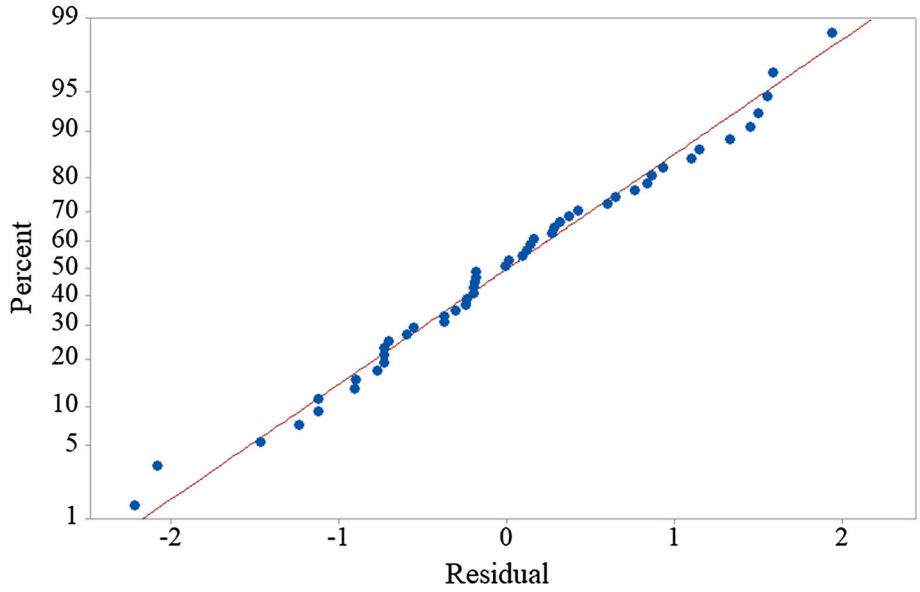

Fig. 7 Normal probability plot of the residuals for the surface roughness

have the most significant influence on the surface roughness of FDM parts.

$$Ra = 22.35 + 9.51A + 2.14C + 2.93D + 7.15E - 0.48AD + 0.68AE + 0.46CE - 3.88A^2 + 8.27D^2 - 1.75E^2 \quad \text{(Eq 4)}$$

For an in-depth study, variable factors were adopted to obtain the interaction effects plot of surface roughness, as presented in Fig. 8. According to the first column of Fig. 8, the surface roughness increases with the rise of the nozzle diameter because the larger nozzle diameter has a lower number of sliced layers for the same height of the part and because both the deposition width and the thickness increase, resulting in the poor surface of the build parts. In contrast to the nozzle diameter, as displayed in the third column of Fig. 8, the surface roughness is insensitive to the extrusion velocity, and it increases slightly with a higher extrusion velocity, possibly because the filament width increases with increased extrusion velocity. Peng (Ref 14) studied the effect of FDM parameters on surface roughness through experimental investigations and found that the choice of filling velocity should be suitable. The

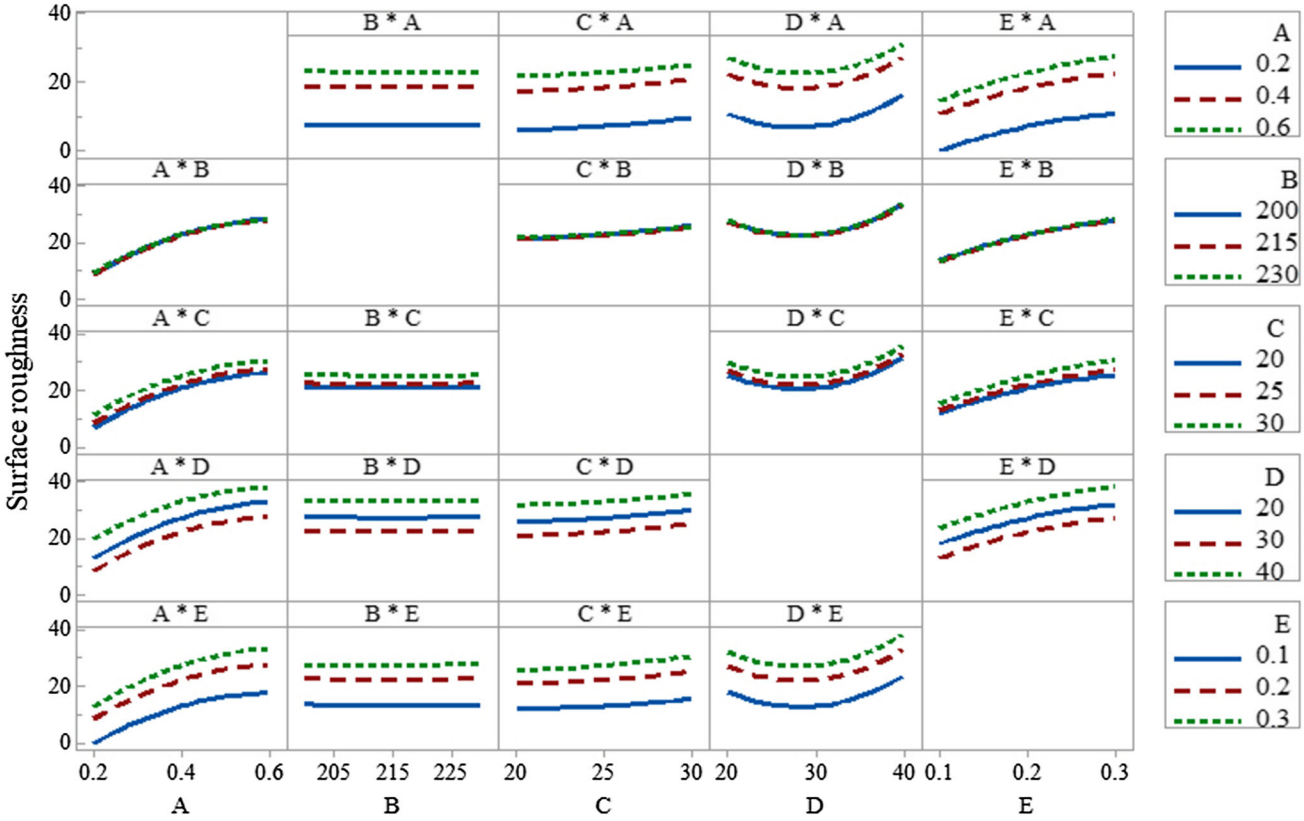

Fig. 8 The influence of parameter interaction on the surface roughness

ultralow velocity causes the lower manufacturing efficiency, possibly causing deposited layers to burn via the searing heat nozzle. The extremely high velocity, however, leads to machine mechanical vibrations, thus reducing component accuracy. As shown in the fourth column of Fig. 8, the roughness decreases first and then increases with increasing filling velocity. The fifth column of Fig. 8 illustrates that the thin layer produced a smoother surface than that of the thick layer. Some results can be found in a previous study (Ref 9, 24).

3.3 Build Time

The ANOVA results of build time are listed in Table 7. The level of confidence is 95%, and the *P* value is less than 0.0001, which shows good applicability of the model. Figure 9 shows the normal probability plot of residual for the response of build time; the plot indicates that the statistics are hardly deviated. The predicted coefficient of 0.9990, similar to the surface roughness, can provide a better evaluation in experiments.

As previously shown, model of build time is presented in Eq 5. According to the *F*-values in Table 7 and the coefficients in Eq 5, the nozzle diameter, liquefier temperature, filling velocity and layer thickness have remarkable linear effects, among which, the nozzle diameter (A) has the greatest effect. Moreover, the quadratic effect of the layer thickness (E^2) and the two level interaction effects of nozzle diameter and layer thickness (AE) have the most significant influence on the build time of forming parts.

$$BT = 1.39 - 1.13A - 0.045B - 0.61D - 0.93E + 0.30A^2 + 0.24D^2 + 0.51E^2 + 0.29AD + 0.46AE + 0.28DE \quad \text{(Eq 5)}$$

Variable factors were chosen to obtain the interaction effects plot of build time, as shown in Fig. 10. According to the first column of Fig. 10, the build time increases with decreasing nozzle diameter, indicating that the extruded filament width is larger when using larger nozzles by the same layer thickness, thereby reducing the required path for the same part and resulting in a shorter required build time. As displayed in the second column of Fig. 10, the build time is insensitive to the liquefier temperature and decreases slightly with greater liquefier temperature because a higher liquefier temperature corresponds to a longer heating time required for printing. In previous research work (Ref 14), the relationship between filling velocity and build time was given; the same variation is obviously observed in the fourth column of Fig. 10. The figure illustrates that, with the other factors fixed, a higher filling velocity shortens the build time required to complete the manufacturing. The fifth column of Fig. 10 demonstrates that the greater the layer thickness, the shorter the processing time,

Table 7 The ANOVA for the build time

Source	SS	DF	MS	*F*-value	*P* value	Remarks
Model	108.4003	20	5.420016	1506.439	< 0.0001	Significant
A	43.73158	1	43.73158	12,154.75	< 0.0001	Significant
B	0.06885	1	0.06885	19.13616	0.0001	Significant
C	0.003012	1	0.003012	0.83709	0.3678	
D	12.74919	1	12.74919	3543.508	< 0.0001	Significant
E	29.18382	1	29.18382	8111.35	< 0.0001	Significant
A^2	0.234973	1	0.234973	65.30845	< 0.0001	Significant
B^2	0.003345	1	0.003345	0.929741	0.3429	
C^2	0.000167	1	0.000167	0.046496	0.8308	
D^2	0.152396	1	0.152396	42.35689	< 0.0001	Significant
E^2	0.664233	1	0.664233	184.6169	< 0.0001	Significant
AB	0.001128	1	0.001128	0.313551	0.5798	
AC	0.001128	1	0.001128	0.313551	0.5798	
AD	2.662278	1	2.662278	739.9534	< 0.0001	Significant
AE	6.872778	1	6.872778	1910.219	< 0.0001	Significant
BC	0.001128	1	0.001128	0.313551	0.5798	
BD	2.81E−05	1	2.81E−05	0.007817	0.9302	
BE	2.81E−05	1	2.81E−05	0.007817	0.9302	
CD	0.005778	1	0.005778	1.605972	0.2151	
CE	0.000253	1	0.000253	0.070354	0.7927	
DE	2.548153	1	2.548153	708.2335	< 0.0001	Significant
Residual	0.104339	29	0.003598			
Lack of fit	0.093189	22	0.004236	2.659289	0.0935	
Total	108.5047	49				

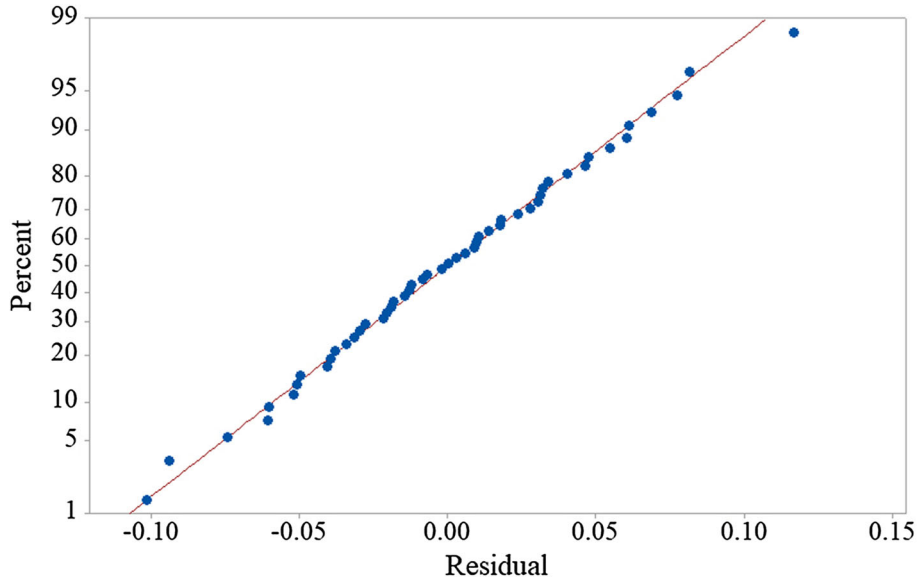

Fig. 9 Normal probability plot of the residuals for the build time

in agreement with a previous study (Ref 14, 19). More layers are required to process the same parts when choosing a thin layer, leading to longer processing time.

3.4 Multiobjective Optimization Process

In theory, the desirable finished parts should not only have the higher tensile strength and surface quality but also lower time cost. In reality, however, these three performance indices are usually conflicting: A combined action of the process parameters leading to higher tensile strength and surface quality possibly results in a higher time cost. Therefore, NSGA-II on controllable variables should be implemented to acquire the optimal combinations of the technological parameters.

3.5 NSGA-II Algorithm

Based on nondominated sorting and sharing, multiobjective evolutionary algorithms have the disadvantages of computational complexity, lack of elitism and the requirement for specifying a sharing parameter. However, NSGA-II reduces all the above weaknesses. NSGA-II is a sorting-based nondominated multiobjective evolutionary algorithm. The NSGA-II algorithm can not only obtain the uniformly distributed Pareto

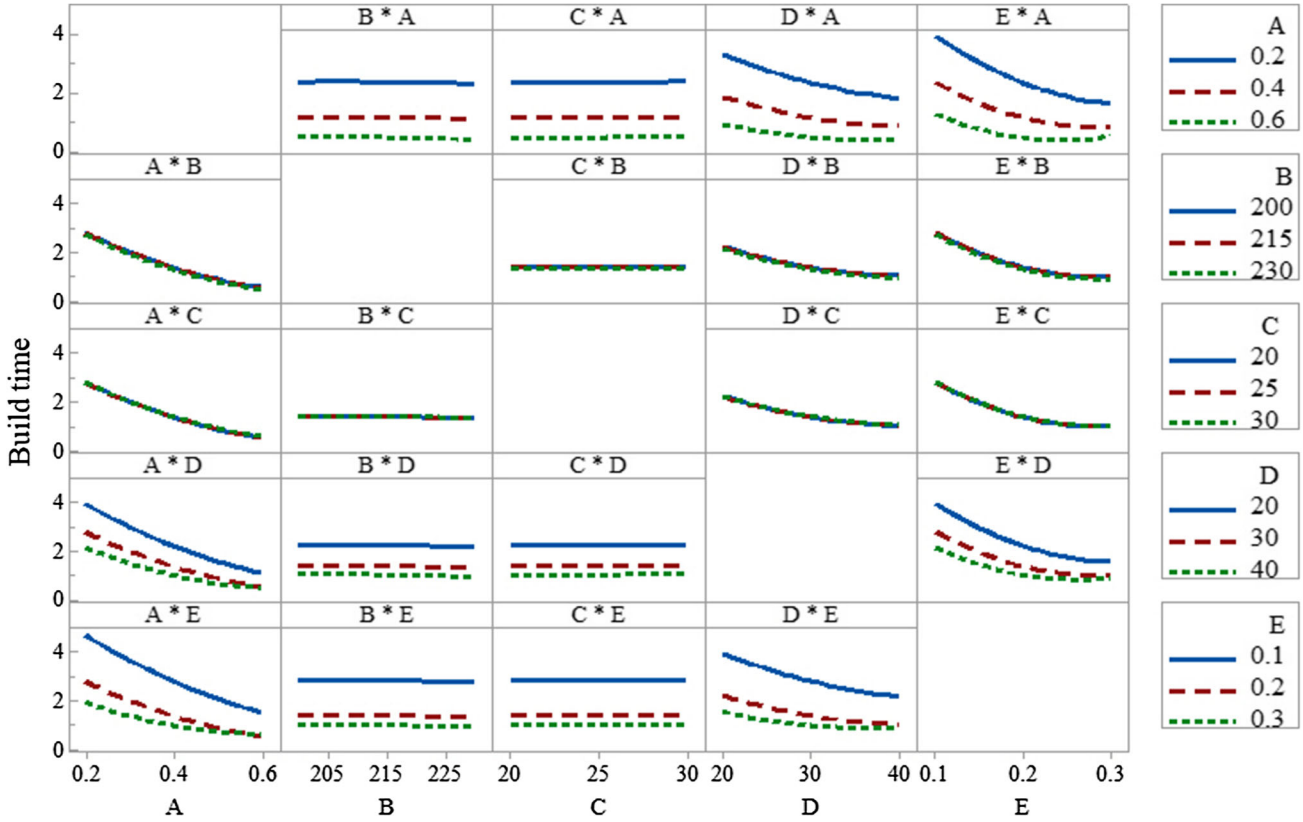

Fig. 10 The influence of parameter interaction on the build time

optimal solution set but also exhibit strong stability and adaptability (Ref 25). Figure 11 illustrates the NSGA-II flowchart. According to this figure, the response surface method is employed in the optimization algorithm to obtain the fitness function. In addition, to generate new groups of crossed and mutated genetic operators, the response surface method is adopted. Finally, the optimization procedure is completed once the iteration condition is satisfied.

3.6 Setting of the NSGA-II Parameters

As shown in Table 8, the objective of the optimization problem is to achieve the optimal process parameters (nozzle diameter, liquefier temperature, extrusion velocity, filling velocity and layer thickness), and the desired results of FDM are to have the maximum tensile strength, minimum surface roughness and minimum build time, all of which are obtained by the ANOVA results.

Table 9 lists the setting for NSGA-II; the program runs in MATLAB R2014b. The implementation of NSGA-II solves the multiobjective optimization problem and obtains the Pareto optimal front.

3.7 Optimization Results

The Pareto optimal front for tensile strength, surface roughness and build time is shown in Fig. 12. Each point represents an acceptable optimum solution, and the corresponding technological parameter can be employed on the basis of the demands of the designers. From Fig. 12, the optimal results are noninferior because there are trade-offs among tensile strength, surface roughness and build time. The implementations of three solutions in the Pareto optimal front confirmed the validity of the optimum results. The confirmation test results obtained by the optimum process parameters are listed in Table 10. From Table 10, the maximum relative error of the tensile strength, surface roughness and build time is 7.95, 13.88 and 6.52%, respectively. By considering the measurement error, the machine constraints and some accidental factors during the experiment process, the error of optimum process parameters is acceptable, indicating that the prediction accuracy of the proposed optimization method is able to meet the requirements of FDM.

4. Summary and Conclusions

In this paper, by applying RSM combined with NSGA-II, the acquisition of the optimized process parameters achieved the maximum tensile strength and the minimum surface roughness and build time. In addition, the solutions are validated by experimental verification. Based on the results, the following conclusions are obtained:

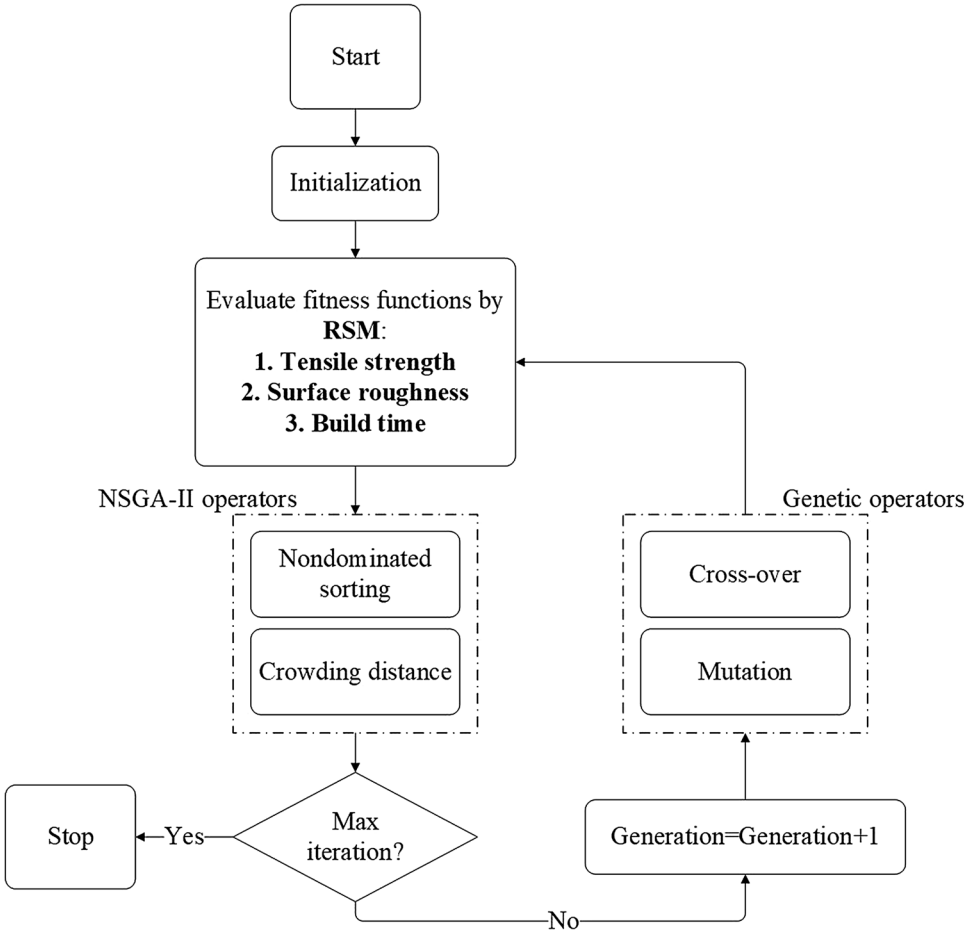

Fig. 11 NSGA-II flowchart

Table 8 Constraints of the parameters and the responses

Name	Goal	Low limit	Upper limit
A: Nozzle diameter	Is in range	0.2	0.6
B: Liquefier temperature	Is in range	200	230
C: Extrusion velocity	Is in range	20	30
D: Filling velocity	Is in range	20	40
E: Layer thickness	Is in range	0.1	0.3
Tensile strength	Maximize	…	…
Surface roughness	Minimize	…	…
Build time	Minimize	…	…

Table 9 NSGA-II parameters settings

Parameter	Value
Population size	100
Maximum iterations	500
Crossover fraction	0.9
Mutation fraction	0.1
Function tolerance	10E−06
Scaling fitness function	Rank

1. On the basis of the ANOVA and *F*-value results, the most effective factors on tensile strength, surface roughness and build time are found to be nozzle diameter and layer thickness. In contrast, liquefier temperature is less effective on surface roughness, and surface roughness is insensitive to the extrusion velocity.
2. Tensile strength and surface roughness increase significantly when using a larger nozzle diameter, high extrusion, filling velocity and thick layers. The increase in the nozzle diameter, filling velocity and layer thickness reduces build time.
3. Based on the results of confirmation experiments, mathematical models developed in this work were tested and verified, which can precisely describe the interrelations between the process conditions. The obtained models can help practitioners achieve a balance among the various mechanical properties, surface finish and build time, thereby reducing effort, time and cost.
4. Although the optimal process parameters were confirmed based only on tensile strength, surface roughness and build time in this study, in practice, the evaluation indicators may involve other parameters, such as dimensional accuracy and material consumption. Moreover, the parts

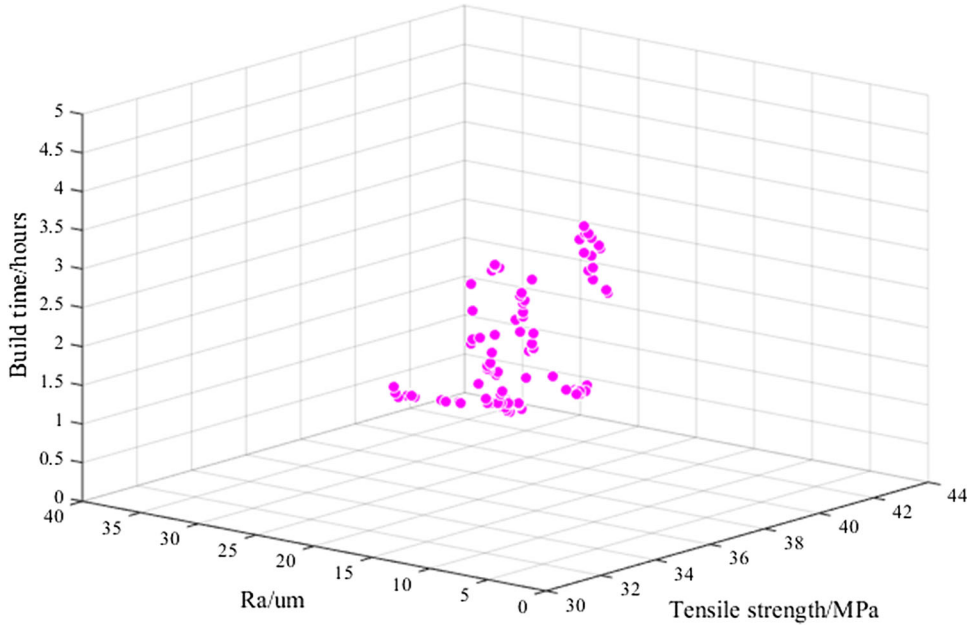

Fig. 12 Pareto optimal front for the tensile strength, surface roughness and build time

Table 10 Results of the confirmation experiments

Nos.		Optimum process parameters					Output responses		
		A	B	C	D	E	TS	SR	BT
1	Optimized	0.21	220.49	20.09	31.86	0.13	33.00	3.35	3.74
	Experimental	0.2	220	20	32	0.1	31.47	3.89	3.93
	Relative error, %						− 4.86	13.88	5.08
2	Optimized	0.39	219.74	20	33.14	0.11	33.91	13.65	2.52
	Experimental	0.4	220	20	33	0.1	36.84	13.91	2.61
	Relative error, %						7.95	1.87	3.45
3	Optimized	0.60	226.19	22.14	30.97	0.19	42.91	26.96	0.49
	Experimental	0.6	225	22	31	0.2	44.75	28.82	0.46
	Relative error, %						4.11	6.45	6.52

required to be fabricated may be more complex in practice. Nevertheless, there is no doubt that the solutions employed in this work have important guiding significance in determining the process parameters.

Acknowledgments

The authors wish to acknowledge the financial support from the National Natural Science Foundation of China (Grant No. 51575442) and the National Natural Science Foundation of Shaanxi Province (Grant No. 2016JZ011).

References

1. S. Ford and M. Despeisse, Additive Manufacturing and Sustainability: An Exploratory Study of the Advantages and Challenges, *J. Clean. Prod.*, 2016, **137**, p 1573–1587
2. J.W. Comb, W.R. Priedeman, and P.W. Turley, *FDM Technology Process Improvements*, University of Texas, Austin, 1994, p 42–49
3. P.F. Jacobs and D.T. Reid, *Rapid Prototyping & Manufacturing: Fundamentals of Stereolithography*, SME Publication, Dearborn, 1992
4. J.J. Beaman, J.W. Barlow, D.L. Bourell, J.W. Barlow, R.H. Crawford, and K.P. McAlea, *Solid Freeform Fabrication: A New Direction in Manufacturing*, Springer, New York, 1997, p 25–49
5. M.E. Sachs, J.S. Haggerty, M.J. Cima, and P.A. Williams, Three dimensional printing techniques, US Patent, 5204055, 1993
6. M. Feygin and B. Hsieh, Laminated object manufacturing (LOM): a simpler process. In: *Proceedings of Solid Freeform Fabrication Symposium, Austin, TX*, p 123–130, 1991
7. O.A. Mohamed, S.H. Masood, J.L. Bhowmik et al., Effect of Process Parameters on Dynamic Mechanical Performance of FDM PC/ABS Printed Parts Through Design of Experiment, *J. Mater. Eng. Perform.*, 2016, **25**(7), p 1–14
8. W.W. Yu, J. Zhang, J.R. Wu et al., Incorporation of Graphitic Nanofiller and Poly(lactic acid) in Fused Deposition Modeling, *J. Appl. Polym. Sci.*, 2017, **134**(15), p 44703
9. C.C. Wang, T. Lin, and S. Hu, Optimizing the Rapid Prototyping Process by Integrating the Taguchi Method with the Gray Relational Analysis, *Rapid Prototyp. J.*, 2007, **13**(13), p 304–315
10. J.W. Zhang and A.H. Peng, Process-Parameter Optimization for Fused Deposition Modeling Based on Taguchi Method, *Adv. Mater. Res.*, 2012, **538-541**, p 444–447

11. A.K. Sood, R.K. Ohdar, and S.S. Mahapatra, Parametric Appraisal of Mechanical Property of Fused Deposition Modelling Processed Parts, *Mater. Des.*, 2010, **31**(1), p 287–295
12. F. Rayegani and G.C. Onwubolu, Fused Deposition Modelling (FDM) Process Parameter Prediction and Optimization Using Group Method for Data Handling (GMDH) and Differential Evolution (DE), *Int. J. Adv. Manuf. Technol.*, 2014, **73**(1-4), p 509–519
13. M.S. Hossain, D. Espalin, J. Ramos et al., Improved Mechanical Properties of Fused Deposition Modeling-Manufactured Parts Through Build Parameter Modifications, *J. Manuf. Sci. E-T ASME*, 2014, **136**(6), p 12
14. A. Peng, X. Xiao, and R. Yue, Process Parameter Optimization for Fused Deposition Modeling Using Response Surface Methodology Combined with Fuzzy Inference System, *Int. J. Adv. Manuf. Technol.*, 2014, **73**(1-4), p 87–100
15. M. Dawoud, I. Taha, and S.J. Ebeid, Mechanical Behaviour of ABS: An Experimental Study Using FDM and Injection Moulding Techniques, *J. Manuf. Process.*, 2016, **21**, p 39–45
16. J. Torres, M. Cole, A. Owji et al., An Approach for Mechanical Property Optimization of Fused Deposition Modeling with Polylactic Acid via Design of Experiments, *Rapid Prototyp. J.*, 2016, **22**(2), p 387–404
17. B.N. Panda, K. Shankhwar, A. Garg et al., Performance Evaluation of Warping Characteristic of Fused Deposition Modelling Process, *Int. J. Adv. Manuf. Technol.*, 2016, **88**(5-8), p 1–13
18. R. Singh, S. Singh, and K. Mankotia, Development of ABS Based Wire as Feedstock Filament of FDM for Industrial Applications, *Rapid Prototyp. J.*, 2016, **22**(2), p 300–310
19. O.A. Mohamed, S.H. Masood, and J.L. Bhowmik, Mathematical Modeling and FDM Process Parameters Optimization Using Response Surface Methodology Based on Q-Optimal Design, *Appl. Math. Model.*, 2016, **40**(23-24), p 10052–10073
20. E. Vahabli and S. Rahmati, Application of an RBF Neural Network for FDM Parts' Surface Roughness Prediction for Enhancing Surface Quality, *Int. J. Precis. Eng. Manag.*, 2016, **17**(12), p 1589–1603
21. B. Standards, Plastics—Determination of Tensile Properties—Part 1: General Principles (ISO 527-1:2012). CEN/TC 249—Plastics
22. The technical data sheet of the PolyPlus-PLA characteristics. http://www.polymaker.com, 2017. Accessed 26 June 2017
23. Ö. Bayraktar, G. Uzun, R.C. Akiroğlu et al., Experimental Study on the 3D-Printed Plastic Parts and Predicting the Mechanical Properties Using Artificial Neural Networks, *Polym. Adv. Technol.*, 2017, **28**, p 1044–1051
24. N.S.A. Bakar, M.R. Alkahari, and H. Boejang, Analysis on Fused Deposition Modelling Performance, *J. Zhejiang Univ. Sci. A*, 2010, **11**(12), p 972–977
25. K. Deb, A. Pratap, S. Agarwal et al., A Fast and Elitist Multiobjective Genetic Algorithm: NSGA-II, *IEEE Trans. Evol. Comput.*, 2002, **6**(2), p 182–197